RSC Advances

ROYAL SOCIETY OF CHEMISTRY

www.rsc.org/advances

One step hydrothermal synthesis of rGO-TiO_2 nanocomposite and its application on Schottky diode: improvement in device performance and transport properties

Mrinmay Das[a], Joydeep Datta[a], Arka Dey[a], Rajkumar Jana[a], Animesh Layek[a, c], Somnath Middya[a,b] and Partha Pratim Ray*[a]

[a.] Department of Physics, Jadavpur University, Kolkata – 700 032, India

[b.] Department of Physics, Bankim Sardar College,Tangrakhali, South 24-paraganas, pin 743329, India

[c.]Department of Physics, Bejoy Narayan Mahavidyalaya, Itachuna, Hooghly-712147, India

*Corresponding Author, e-mail:partha@phys.jdvu.ac.in;

Phone: +91-9475237259; Fax: +91-3324138917

Abstract

The presence of a Schottky barrier (SB) at a metal-semiconductor (MS) interface is of paramount importance to numerous application fields. In this report, we demonstrate the performance comparison of schottky diodes fabricated with TiO_2 and rGO-TiO_2 nanocomposite, in contact with aluminium. From forward I-V characteristics, important diode parameters i.e. rectification ratio, ideality factor, series resistance and barrier height were obtained. Photoresponse comparison of the diodes has also been done. It was found that rGO-TiO_2 based junction showed improved performance. The rectification ratio increased by ~94% and barrier height was lowered by ~10%, under dark condition. For better realization of the junction, here we provide an insight into the carrier transport properties with the help of space charge limited current (SCLC) theory. After introducing graphene, carrier mobility and carrier concentration increased by 64% and 21% respectively, while diffusion length is found to be improved by 13.4%. These results illustrate that rGO incorporation has led to a much improved carrier transport and electron hole separation. Due to greater light absorption, the improvement in diode parameters and transport properties were even better when the device was subjected to irradiation.

Keywords: rGO-TiO_2 nanocomposite, thin film, metal-semiconductor junction, photoresponse, transport properties

1. Introduction

Graphene, the two dimensional wonder material composed of sp^2 hybridized carbon atom, has attracted huge interest in recent times due to its fascinating properties[1]. It possess this remarkably unique combination of excellent conductivity, high carrier mobility at room temperature, optical transparency over a wide wavelength region and a flexible yet robust structure as well[2,3]. Equipped with these qualities, graphene has entered a broad field of potential application such as electronic devices, nano-composites, photosensors etc[3]. Moreover, this excellent material can be obtained from graphite, which is cheap and abundant. The fact that the specific surface area of graphene is 2630 m^2/g,[2] only adds to its case as a potential candidate for electronic applications. This high surface area enables higher absorption of light and greater interfacial contact area, which serves its use as a support material, even in very small amount.

In realm of electronics, graphene has already seen many applications in Schottky devices, a very important part in today's high tech electronics due to its low turn on voltage and high speed switching[4]. It is seen that several factors like short carrier lifetime, high recombination rate, quality of the interface, band gap of the material have profound impact on the performance of a Schottky barrier diode (SBD)[5,6]. Also, there have been other issues like cost and toxicity of materials. So it has been desirable for long to overcome these problems as much as possible and many semiconductor materials have been studied for this purpose. CdS, ZnS, ZnO, TiO_2, CdTe, CdSe are few of those. Among them, TiO_2 has been widely used due to its promising features like tunable microstructure, chemical stability, non-toxicity, easy availability and low cost[7]. Despite all this attributes, high recombination rate of electrons and holes has remained one of the main concerns for device application of TiO_2[8]. Moreover, with its 3.2 eV electronic band gap, TiO_2 is only sensitive to the light wavelengths below ~380 nm which belong to the UV region[9]. Proper utilization of solar energy is possible if a suitable lower band gap can be achieved, which is desirable for photovoltaic applications. Also, it would be excellent if the high recombination rate can be taken care of. According to earlier reports, in comparison to pure TiO_2, carbon nanotube TiO_2 or graphene TiO_2 has few advantages, namely enhanced electron-hole pair (EHP) separation and extended visible light absorption[10,11]. The heterojunction formed between graphene and TiO_2 separates the photo

generated EHPs in TiO_2 with electron injecting into graphene, thus suppressing recombination[10,12]. Considering these factors some investigation on graphene TiO_2 composite has been done. But, an in depth analysis of the schottky diode parameters and charge transport properties through a metal/rGO-TiO_2 junction have received little attention. With the recent emergence of novel Schottky barrier based nanoelectronics, a detail perceptive of this interface is in high demand. These led to our great interest in studying the graphene-TiO_2 nanocomposite based Schottky diode and its transport mechanism, compared to the one fabricated with pure TiO_2.

However, high purity graphene is incredibly difficult to achieve. So, reduced graphene oxide (rGO) is used more often, which can be produced using the well known Hummers method[13,14], followed by a reduction strategy. We also followed the same path for producing rGO. In this work, we present the performance comparison of TiO_2 nanoparticles and rGO-TiO_2 composite in schottky barrier diode. Structural and optical characterization of the samples was performed. Schottky device of metal/semiconductor/TCO configuration was fabricated for both materials and important characteristic parameters like rectification ratio, ideality factor, series resistance and barrier height were obtained from current-voltage (I-V) measurements. Aluminium was chosen as the metal contact. We also observed the device performance under light to find out the changes in photo response, induced by rGO integration into TiO_2 matrix. To explain the changes, carrier transport properties were analyzed by standard space charge limited current (SCLC) theory.

2. Materials and methods

2.1. Synthesis of TiO_2 and rGO-TiO_2

Graphene oxide (GO) was prepared by modified hummers method[13-15]. 2 g of graphite flakes was mixed with conc. H_2SO_4 and phosphoric acid (100 mL: 15 mL). Under vigorous stirring for 1 day, 10 g of $KMnO_4$ was added gradually. 100 mL ice water and 10 mL H_2O_2 solution (30%) was slowly added to the mixture, forming a brown color. Then, the mixture was washed with 10% HCl (aq.) and deionized water in order. Finally, the resulting sample was dried under vacuum condition to get GO powder.

To synthesize TiO_2 nanoparticles, hydrothermal process was utilized. 0.1 M $TiCl_4$ and 0.1 M NaOH aqueous solution was prepared in two separate beakers. NaOH was added

dropwise to the $TiCl_4$ solution until pH became 6-7. The mixture was kept under vigorous stirring for 6 h and then transferred to a Teflon lined autoclave, which was heated at 160 °C for 24 h. The resulting product was then washed thoroughly with distilled water and ethanol, followed by vacuum drying. A white powder was obtained and separated in two parts. One was retained as synthesized, while the other part was used to obtain rGO-TiO_2 nanocomposite.

A well dispersed solution of GO in water (0.5 mg/mL, 10 mg: 20 mL) was prepared by ultrasonication for 6 h. The suspension was subjected to hydrazine treatment to obtain reduced graphene oxide (rGO). 5 mL hydrazine hydrate was added to the solution and kept under vigorous stirring for 8 h. A black precipitate appeared, which was washed several times with ethanol and distilled water. After washing thoroughly, heating was done to collect the desired rGO powder, subsequently divided in two parts. One part was taken for characterization. The 2nd part was introduced to TiO_2 matrix for producing rGO-TiO_2 nanocomposite. As prepared TiO_2 was added to the rGO (TiO_2: rGO=30:1, weight ratio) dispersion and stirred for 8 h. Thereafter a hydrothermal reaction was carried out at conditions similar to that for TiO_2. As before, the resultant solution was washed and dried to obtain the rGO-TiO_2 nanocomposite as final product. Also, samples with weight ratio 15:1 and 50:1 were prepared in same process to see their diode behavior. All the AR-grade reagents were purchased from Merck.

2.2. Fabrication of ITO/ TiO_2 /Al and ITO/ rGO-TiO_2 /Al based Schottky diode

To fabricate our desired Schottky devices of ITO/ TiO_2 /Al and ITO/ rGO-TiO_2 /Al configuration, two indium tin oxide (ITO) coated glass substrates was cleaned with soap solution, acetone, ethanol and distilled water sequentially in an ultrasonic bath. Then well dispersed solution of the samples (TiO_2 and rGO-TiO_2) were prepared in ethanol medium and eventually spin coated onto the ITO coated glass at 1200 rpm for 2 minutes, followed by drying of the film. The film thickness was ~1 μm, measured by surface profiler. Aluminium (metal) was chosen as the rectifier contact and deposited on the films by thermal evaporation technique to construct metal-semiconductor junction. The effective diode area was 7.065 x 10^{-2} cm^2, as maintained by shadow mask.

2.3. Characterization

The morphology of the as synthesized graphene sheets, TiO_2 nanoparticles and rGO-TiO_2 composite was assessed by a field emission scanning electron microscope (FESEM) FEI Inspect F50. Further morphological characterization was done by a JEOL make transmission electron microscope (TEM). To identify the crystalline phase of the as synthesized samples, powder X-ray diffraction experiment was carried out using Bruker made D8 X-Ray diffractometer, with Cu Kα radiation(λ=1.5418A^0). A FTIR-8400S Spectrophotometer of Shimadzu was used to obtain the Fourier transform infrared spectroscopy (FTIR). Raman spectra for the samples were collected at room temperature by Renishaw inVia micro Raman Specroscopy (Excitation: 514 nm Ar ion Laser)**.** X-ray photoelectron spectroscopy (XPS) measurements were carried out using a Specs Spectrometer with an Al monochromator (1486.6 eV) and a Mg K_α source (1253.6 eV) under a vacuum of < 10^{-9} Torr. The spectrum was deconvoluted by using CASA XPS software. Thermogravimetric analysis (TGA) was done by METTLER TOLEDO TGA/SDTA -851-e. UV-vis absorption spectra were recorded using 2401PC spectrophotometer of Shimadzu. Current voltage measurements were studied by a Keithley 2400 sourcemeter interfaced with computer. For BET analysis, N_2 gas adsorption study was performed at 77 K with the desolvated form of TiO_2 and rGO-TiO_2 maintained by a liquid-nitrogen bath, with pressures ranging from 0 to 1 bar using a Quantachrome Autosorb-iQ adsorption instrument. A highly pure quality of N_2 (99.9999%) is used to analyse without any further purification.

3. Results and discussion

Fig. 1 shows the FESEM images of as prepared samples. Well dispersed graphene sheets can be easily distinguished from the Fig. 1(a). The morphology of TiO_2 particles is spherical and of nano range, as can be seen from Fig. 1(b). It is observed in Fig. 1(c) that TiO_2 nanoparticles are grafted nicely onto the graphene sheets, achieved through Ti−O−C bonding between TiO_2 and rGO during the hydrothermal process[10]. But, there are some agglomerations of TiO_2 at places, which can diminish the benefits of large interfacial area between the particles and sheets to some extent. On the other hand, it is well known that layers of rGO have the tendency to aggregate due to strong van der Waals interaction[16]. This was ably prevented by TiO_2 particles deposited on rGO sheets.

The TEM images of the materials are shown in Fig. 1(d) and Fig. 1(e). Fig. 1(d) shows the TiO_2 particles, which are found to be 20-25 nm in size. This is in well harmony with the particle size obtained from scherrer's estimation. Decoration of TiO_2 nanoparticles on the graphene sheet is clearly depicted in Fig. 1(e), which gives them a good contact and eventually increases charge transport properties.

The XRD patterns of rGO, TiO_2 and rGO-TiO_2 nanostructures are shown in Fig. 2(a). The characteristic peak (002) for reduced graphene oxide can be seen around $2\theta = 24°$ to 25° [16, 17]. The spectrum for rGO is separately shown in supplementary section (Fig. S1). The diffraction spectrum recorded for TiO_2 nanoparticles showed peaks of anatase phase TiO_2 nanoparticles at $2\theta = 25.37°$, 37.07°, 37.89°, 38.58°, 48.07°, 53.97°, 55.1°, 62.71°, 68.78°, 70.41° and 75.08° corresponding to the (101), (103), (004), (112), (200), (105), (211), (204), (116), (220) and (215) diffraction planes respectively. The results are supported by jcpds card no 84-1286. The XRD spectrum for rGO-TiO_2 nanocomposite did not show any changes from TiO_2 either. Notably, the broad diffraction peak of graphene disappeared in the composite spectrum. This suggests that the rGO peak was overlapped by the main (101) peak of TiO_2, may be due to small amount of graphene.

Williamson–Halls' estimation has been employed to measure the average particle size of TiO_2. For this, only the major peaks were considered. The particle size was estimated at 25 nm from y axis intercept of the $\beta_r \cos\theta$ vs. $\sin\theta$ (Fig. 2(b)) plot:

$$\boldsymbol{\beta_r \cos\theta = \frac{K\lambda}{D} + \mu \sin\theta} \qquad \textbf{(1)}$$

Fig. 2(c) represents the FTIR spectra of the samples. Both spectra showed low frequency band around 670 cm^{-1}, which was assigned to the presence of Ti-O-Ti bond[10,18]. The stretching vibrational peak for Ti-O-Ti bond was observed just below 1000 cm^{-1} [7]. The broad peak in the range 2700-3700 cm^{-1} can be ascribed to the O-H stretching vibration of the hydroxyl groups on the surface of TiO_2[7,10]. The absorption around 1640 cm^{-1} was also due to hydroxyl groups of molecular water[8,19], which means TiO_2 nanocrystal easily absorbs water in the air. A relatively stronger peak was observed at 2357 cm^{-1}. This was due to CO_2 molecules being adsorbed on TiO_2 surface from atmosphere[7]. As for the rGO-TiO_2 spectra, the peak at 795 cm^{-1} was attributed to the presence of Ti-O-C bonds, which confirms that, during hydrothermal reaction, a strong chemical bond was formed between graphene and TiO_2 nanoparticles[10]. Another noteworthy observation was the existence of a peak at 1585

cm^{-1} for rGO-TiO_2 composite, while it was absent in pure TiO_2. This is the signature for skeletal vibration of graphene sheets[10, 20, 21]. The characteristics peaks of GO at 1052 cm^{-1}, 1720 cm^{-1} and 1220 cm^{-1} due to C-O stretching, C-OH stretching and C=O stretching respectively, were missing in the spectrum[22]. That means most of the oxygen containing functional groups were decomposed. However, a weak band at 1435 cm^{-1} (carboxyl C-O) implies that partial hydroxyl functionalities were still present in rGO[23]. These results demonstrate that GO was well reduced to graphene sheets and successfully functionalized with TiO_2 nanoparticles.

Raman spectroscopy has been a very useful tool for characterization of graphitic materials for long time. Fig. 2(d) shows the raman spectra of TiO_2 and rGO-TiO_2 nanocomposite. Raman lines for E_g, B_{1g}, A_{1g}, or B_{1g} modes of TiO_2 anatase phase were observed in both[10]. The spectra of rGO-TiO_2 shows a D band peak at 1350 cm^{-1} and another peak of G band at 1588 cm^{-1}, representing typical characteristics of rGO[24]. Moreover, the intensity ratio of the D and G band i.e. I_D/I_G ratio was measured to be 0.89. This value is pretty close to previously reported value[24], further cementing the successful synthesis of rGO-TiO_2 composite by hydrothermal technique. This was due to the decrease in the sp^2 domain size of carbon atoms and the reduction of sp^3 to sp^2 carbon during the solvo-thermal process.

XPS is a powerful technique to determine the reduction level and nature of chemical bonding in rGO or rGO-TiO_2 composite [25]. Fig. 3 provides the survey and elements XPS spectra of GO and rGO-TiO_2 composite. The rGO-TiO_2 composite mainly shows carbon, oxygen and titanium species in the survey spectrum in Fig. 3(a). Fig. 3(b) shows a high-resolution spectrum of the Ti 2p peak, which consists of a doublet with peaks at 458.5 eV and 464.2 eV, corresponding to the Ti $2p_{3/2}$ and Ti $2p_{1/2}$ core levels of TiO_2, respectively [26]. The splitting width of 5.7 eV is in well accordance with earlier report [27]. The deconvoluted C 1s spectra of GO is shown in Fig. 3(c), showing the presence of four type of carbon bonds: C–C (284.5 eV), C–O (285.3 eV), C=O (286.4 eV), and O–C=O (288.6 eV) [27]. Compared to GO, intensity of the peaks related to the oxidized carbon in rGO-TiO_2 decreases radically in Fig. 3(d), which indicates the successful reduction of GO.

TGA is an effective analytical technique to analyze the stability of the materials and to determine the ratio of the components in a composite. In Fig. 4, the TGA curves of TiO_2 and rGO-TiO_2 are depicted. TiO_2 shows a loss of about 1% upto 100 °C, while the curve for

rGO-TiO_2 shows 0.45% weight loss from 30 °C to 100 °C, due to loss of adsorbed water. After that, a weight loss of 3.15% upto 515 °C is observed, which can be ascribed to the oxidation of rGO. Beyond this temperature, the composite is relatively stable and shows little weight loss. The residue is associated with the TiO_2 nanoparticles. So, from TGA analysis of rGO-TiO_2 curve, it can be estimated that the content of graphene in the composite is about 3.2%. This is in well agreement with the designed value.

Adsorption analysis of TiO_2 and rGO-TiO_2 with N_2 at 77 K exhibits typical type-II isotherm, suggesting only surface adsorption (Fig. 4(b)) and the final uptake found as 201 cc/g and 240 cc/g respectively for TiO_2 and rGO-TiO_2. Using BET equation, 1/[W{(Po/P) - 1}] is calculated at different relative pressure. In the micropore region of N_2 adsorption isotherm, plot fitting method is used to obtain BET surface area. Calculated surface area for TiO_2 and rGO-TiO_2 are 76.063 m^2/g and 98.845 m^2/g respectively. So, the surface area for the graphene based composite increased to a good extent, enabling better interfacial contact and light absorption.

The absorption property and band gap of the materials was studied by UV-vis absorption analysis (Fig. 5). Absorption spectrum for rGO is given in the inset. A peak at 271 nm corresponding to π- π* transition of aromatic C-C bond can be seen, whereas this peak appears at around 234 nm for GO. This red shift indicates the reduction of GO and restoration of C=C bonds in rGO sheets[22,28]. From the spectra of pure TiO_2 and rGO-TiO_2 nanocomposite, the enhanced absorption of the later is clear, which is attributed to the presence of graphene. This wider range of absorption should improve the utilization of light and hence photoresponse. Band gap of the materials were calculated using the equation (2)[7]

$$\boldsymbol{E_{bg} = \frac{1240}{\lambda}(eV)} \qquad \textbf{(2)}$$

Where, E_{bg} = band gap of the material, λ= maximum wavelength in nm. The band gap was estimated as 2.96 eV and 1.87 eV for as synthesized TiO_2 and rGO-TiO_2 respectively. These values show that successful incorporation of graphene has significantly lowered the band gap, which is of great importance for various applications.

To observe the current voltage characteristics two devices of Al/TiO_2/ITO and Al/rGO-TiO_2/ITO configuration was fabricated. For characterization, a bias voltage varying from -1 V to +1 V was applied between Al electrode and the substrates. I-V measurements were recorded with a Keithley 2400 sourcemeter under dark and photo illumination. Obtained

result is presented as I vs V curve in Fig. 6. log I vs V graph is shown in inset. The graphs for dark and light are plotted in same scale for comparison.

As the plots illustrate, both device portrayed good rectifying behaviour, which is the signature of a Schottky diode. Higher current was recorded for the rGO-TiO_2 device. Remarkably, even the dark current showed by rGO-TiO_2 Schottky device was greater than the photocurrent of TiO_2 based one. The on/off current ratio for the rGO-TiO_2 diode was 35 at dark and 85 at photo condition, which was significantly greater than the values of 18 and 36 obtained for its counterpart. So, it is clear that graphene composited TiO_2 make for a better rectifying device than pure TiO_2. The room temperature conductivity was estimated to be 3.8 x 10^{-6} S/cm and 4.8 x 10^{-6} S/cm for the TiO_2 diode, under dark and light respectively. For our composite based device these values were 7.6 x 10^{-6} and 1.3 x 10^{-5}, indicating enhanced conductivity. This increase for the composite is attributed to the high conductivity of graphene and its good contact with the TiO_2 nanoparticles. For investigating photoresponse, we measured the transient photocurrent of the devices under an illumination of 80 mW/cm^2 at bias voltage 1V, which is represented in Fig. 7. Dark currents were subtracted in order to compare the photosensitivity. The diode fabricated with pure TiO_2 exhibited photosensitivity of the order 1.26. In presence of graphene, that value increased appreciably by ~42% to 1.77.

To further analyze the diodes, thermionic emission theory was employed. Current voltage dependence of a Schottky diode is given by the equation[29]:

$$\boldsymbol{I = I_0\left[exp\left(\frac{qV}{nkT}\right) - 1\right]} \qquad \textbf{(3)}$$

Where, I is forward current, I_0 the reverse saturation current, V the applied bias, q the electronic charge, *k* the Boltzman constant and T is the absolute temperature. n is the ideality factor, a constant taken into account for non-ideal behaviour of diode. I_0 can be represented by [29]:

$$\boldsymbol{I_0 = AA^{*}T^{2}\, exp\left(\frac{-q\phi_b}{kT}\right)} \qquad \textbf{(4)}$$

Where, A, A^* and ϕ_b are effective diode area, Richardson constant and Schottky barrier height respectively. Effective diode area was 7.065 x 10^{-6} m^2 and Richardson constant was considered as 24 A/cm^2K^2 [30]. Important parameters like ideality factor, series resistance, barrier height of the Schottky diode was measured using the equations [29]:

$$\frac{dV}{d\ ln(I)} = \frac{nkT}{q} + IR_s \qquad (5)$$

$$H(I) = V - \left(\frac{nkT}{q}\right) ln\left(\frac{I}{AA^*T^2}\right) \qquad (6)$$

and

$$H(I) = IR_S + n\phi_b \qquad (7)$$

Where, R_S is the series resistance of the diode. The dV/d ln(I) vs I graphs for dark and photo condition are portrayed in the Fig. 8. Series resistance and ideality factor was determined from the slope and y axis intercept, respectively. Fig. 8 also depicts the H(I) vs I plots, which is linear and y axis intercepts of these plots give the barrier height. The obtained values of ideality factors are listed in the table 1, implying deviation from ideal behaviour. This indicates the presence of inhomogenities of Schottky barrier height and existence of interface states, and series resistance [31]. Upon light irradiation the values approached to unity for both devices, but there was no obvious relation between the active materials and ideality factor. Series resistances of the fabricated devices under dark and photo condition, as obtained from the above mentioned graphs, are also shown in Table 1. For further verification, series resistance was also calculated from H(I) vs I curve. It is evident from the table that both methods returned more or less the same result. Notably, the value of R_S reduced drastically for the rGO-TiO_2 diode compared to the other device. This large difference in series resistances of the junctions duly explains the higher current displayed by the composite device. Barrier heights of the Schottky diodes were 0.47 eV and 0.42 eV for TiO_2 under dark and photo condition respectively, while they were calculated to be 0.42 eV and 0.37 eV for rGO-TiO_2 (Table 1). Again, a striking feature is noticed here i.e. barrier potential for the later under dark is equal to that of the former under light. These values suggest that presence of graphene has led to a lower turn on voltage. So, the synthesized rGO-TiO_2 is expected to be a better candidate than pure TiO_2 for fast switching device application. The I-V curves (Fig. S2), dV/d ln(I) vs I and H(I) vs I graphs (Fig. S3), and diode parameters (Table S1) for the composites with weight ratio 15:1 and 50:1 are given in supplementary section. It is seen that the device performance of rGO-TiO_2 improved for all the cases, compared to pure TiO_2.

According to the above results, graphene has caused significant improvement in various parameters of our fabricated Schottky barrier diode. Graphene has an electron mobility of 10^4 cm^2/V s at room temperature[2]. So, it is expected to enhance the electron

transfer and EHP separation of the composite. To verify this impact of graphene and get a better insight of the carrier transport mechanism, the I-V curves were further analyzed by evaluating mobility, lifetime and diffusion length of the carriers. Standard SCLC theory was employed for this purpose. Log I vs log V graph is plotted in Fig. 9(a) and Fig. 9(b), where three distinct regions with different slope can be seen. At low bias (region I), the current voltage characteristics obeys ohmic nature, beyond that it is governed by space charge limited current upto some point (region II) and then it follows $I \alpha V^n$ (region III). Effective carrier mobility was estimated from SCLC region of I vs V^2 graph (Fig. 9(c) and Fig. 9(d)). Effective carrier mobility was obtained from the Mott-Gurney equation for space-charge limited-current (SCLC) [32,33]:

$$\boldsymbol{I = \frac{9\mu_{eff}\,\varepsilon_0\varepsilon_r A}{8}\left(\frac{V^2}{d^3}\right)} \qquad \textbf{(8)}$$

where ε_0 is the dielectric permittivity of vacuum, ε_r the dielectric constant of the semiconductor (earlier reported value of ε_r= 50 was taken)[34], μ_{eff} the effective electron mobility and d the thickness of the film (about ~800 nm for our device). The following equations were further used to extract lifetime (τ) from log I vs log V graph (Fig. 12) and diffusion length (L_D) of the charge carriers[33]

$$\boldsymbol{\tau = \frac{9\varepsilon_0\varepsilon_r A}{8d}\left(\frac{V}{I}\right)} \qquad \textbf{(9)}$$

$$\boldsymbol{L_D = \sqrt{2D\tau}} \qquad \textbf{(10)}$$

Where, D is the diffusion coefficient and can be calculated from Einstein-Smoluchowski equation[33]:

$$\boldsymbol{\mu_{eff} = \frac{qD}{kT}} \qquad \textbf{(11)}$$

K is the Boltzman constant and T is temperature in Kelvin.

Apart from this, the carrier concentration (N) near the junction of the devices was estimated by [35]:

$$\boldsymbol{N = \frac{\sigma}{q\mu}} \qquad \textbf{(12)}$$

Estimated values of effective carrier mobility, carrier lifetime, carrier concentration and diffusion length are presented in Table 2.

From the Table 2, for graphene incorporated TiO_2, mobility was far higher than pure TiO_2. For rGO-TiO_2, in dark condition, mobility of the carriers was higher by ~64%, whereas under light it increased by a mammoth ~121%. Also, an improvement of ~21% and ~25% in carrier concentration was observed for dark and illuminate condition repectively. Charge carriers in the graphene composite based diode had reasonably greater diffusion length compared to those in the other device. More precisely, in presence of graphene the diffusion length increased by ~13.5% under dark and ~30% under photo condition. Clearly, the high mobility of graphene and its encouraging contribution in light absorption capability are reflected in these results. So, from SCLC mechanism, we successfully obtained the parameters which justify the presumed effect of rGO.

To further verify these conclusions derived from our theoretical approach of SCLC, few measurements for analyzing the electron transfer kinetics were performed. Fig. 10(a) shows the cyclic voltammograms of the as prepared thin films TiO_2 and rGO-TiO_2. Anodic and cathodic peaks for both samples are detectable. The peak to peak separation for the rGO-TiO_2 is smaller than TiO_2. Another important observation is that the composite gave almost 1.8 fold higher anodic current density. Notably, our I-V measurements under dark condition also returned quite similar pattern for two films, where the current was higher by 1.6 fold for rGO-TiO_2. So, the composite sample demonstrated considerably enhanced electron transfer kinetics, which is due to the highly conductive graphene sheets.

After being irradiated, semiconductors emit photons upon electron hole recombination, which results in photoluminescence (PL). Therefore, to account for the higher photocurrent displayed by the graphene TiO_2 composite, photoluminescence was employed. Fig. 10(b) depicts the room temperature PL spectra of pure TiO_2 and rGO-TiO_2. An emission quenching of TiO_2 is observed in the composite, representing increased photogenerated electron transfer from TiO_2 to rGO. Hence, the EHPs could be more efficiently separated and inhibited from being recombined.

So, it can be suggested that, the improvement in current, photosensitivity and other parameters of rGO-TiO_2 Schottky junction resulted from graphene. This effect can be explained physically by following: (a) Much higher mobility and greater diffusion length i.e. improved EHP separation. In normal TiO_2, electrons have more possibilities to be recombined by hole while moving through the film. In the composite, graphene sheets construct an extensive 2D π- π conjugation network penetrating into TiO_2 matrix. Moreover,

conduction band of TiO_2 is at -4.2 eV and work function of graphene is in the range 4.42-4.5 eV [36,37]. It encourages possible electrons transfer from conduction band of TiO_2 to graphene (schematic diagram shown in Fig. 11). The electrons move through the graphene sheets and gets collected before being recombined. Thus electrons in this network get higher mean free path and contributes to larger current. (b) Enhanced absorption of light by rGO-TiO_2. Introduction of graphene led to a wider range of absorption. This is attributed to the high surface area of graphene sheets. As a result more charge carriers were generated upon light soaking (Table-II), thus increasing the photocurrent significantly. In our graphene-TiO_2 composite, graphene acts more like many extended current collectors penetrating into the TiO_2 matrix. Electrons can travel longer distance and finally gets collected by external circuit.

4. Conclusion

In conclusion, hydrothermal method was employed to synthesize TiO_2 and rGO-TiO_2 hybrid nanoparticles with different weight ratio of rGO. Comparative studies revealed the supremacy of rGO-TiO_2 based SBD for all the cases. The rectification ratio increased significantly and turn on voltage was lowered. The improvement in diode parameters was explained by evaluating the carrier transport mechanism through the metal-semiconductor junction. SCLC theory was used to extract mobility, carrier concentration and diffusion length of carriers, which reflected superior transport properties of the rGO-TiO_2 schottky device. Increased light absorption in the presence of graphene ensured an even better performance under illumination. The properties of graphene were validated to contribute to the enhanced charge separation and transportation. In light of these results, we infer that rGO-TiO_2 is a promising alternative over TiO_2 for better rectification and fast switching device application. Moreover, the overall picture emerging from present study shed light on the carrier transport across MS interface and can open up the prospect for further improvement in graphene based SBDs by optimizing the graphene content, film and interface quality.

5. Acknowledgements

The author would like to thank Department of Science and Technology, Government of India for their fellowship under INSPIRE AORC program. The support of PURSE and

FIST program of Department of Science and Technology, Government of India is also acknowledged.

References:

1. C. N. R. Rao, A. K. Sood, K. S. Subrahmanyam and A. Govindaraj, *Angew. Chem., Int. Ed.*, 2009, **48,** 7752-7777.

2. S. Sun, L. Gao and Y.Liu, *Appl. Phys. Lett.,* 2010, **96,** 083113(1-3).

3. Y. F. Li, W. Yang, Z. Q. Tu, Z. C. Liu, F. Yang, L. Q. Zhang and R. Hatakeyama, *Appl. Phys. Lett.,*2014, **104**, 043903(1-4).

4. I. Missoum , M. Benhaliliba, A. Chaker , Y.S. Ocak , C.E. Benouis, *Synt. Met.*, 2015, **207**, 42-45.

5. J. Vobecky´, P. Hazdra, V. Zahlava, A. Mihaila and M. Berthou, *Solid State Electron.,* 2014, **94**, 32‑38.

6. J. Osvald, *J. Appl. Phys.,* 1999, **85(3)**, 1935‑1942.

7. M. R. Hasan, S. B. A. Hamid, W. J. Basirun, Z. Z. Chowdhury, A. E. Kandjanib and S. K. Bhargavab, *New J. Chem.,* 2015, **39**, 369-376.

8. L. L. Tan, W.J. Ong, S. P. Chai and A. R. Mohamed, *Nanoscale Res. Lett.,* 2013, **8:465**(1-9).

9. S. Malato, P. F. Ibáñez, M.I. Maldonado, J. Blanco and W. Gernjak, *Catal. Today,* 2009, **147(1)**, 1–59.

10. X. Pan, Y. Zhao, S. Liu, C. L. Korzeniewski, S.Wang and Z. Fan, *ACS Appl. Mater. Interfaces*, 2012, **4 (8)**, 3944–3950.

11. K. Woan, G. Pyrgiotakis and W. Sigmund, *Adv. Mater.*, 2009, **21**, 2233-2239.

12. Q. Xiang, J. Yu and M. Jaroniec, *Nanoscale*, 2011, **3**, 3670-3678.

13. W. S. Hummers Jr and R. E. Offeman, *J. Am. Chem. Soc.*, 1958, **80(6)**, 1339.

14. N.M. Huang, H.N. Lim, C.H. Chia, M.A. Yarmo and M.R. Muhamad, *Int. J. Nanomed.*, 2011, **6**, 3443‑3448.

15. D. C. Marcano, D. V. Kosynkin, J. M. Berlin, A. Sinitskii, Z. Sun, A. Slesarev, L. B. Alemany, W. Lu and J. M. Tour, *ACS Nano*, 2010, **4(8)**, 4806‑4814.

16. S. D. Perera, R. G. Mariano, K. Vu, N. Nour, O. Seitz, Y. Chabal and K.J. Balkus, *ACS Catal.*, 2012, **2(6)**,949–956.

17. K. Zhang, Y. Zhang and S. Wang, *Sci. Rep*., **3:3448**, 1-7.

18. N. Yang, J. Zhai, D. Wang, Y. Chen and L. Jiang, *ACS Nano*, 2010, **4 (2)**, 887–894.

19. L. Pan, J. J. Zou, S. Wang, X. Y. Liu, X. Zhang and L. Wang, *ACS Appl. Mater. Interfaces*, 2012, **4(3)**, 1650–1655.

20. C. Nethravathi and M. Rajamathi, *Carbon*, 2008, **46**, 1994-1998.

21. K. Zhou, Y. Zhu, X. Yang, X. Jiang and C. Li, *New J. Chem.*, 2011, **35**, 353-359.

22. Y. Zhang, H. L. Ma, Q. Zhang, J. Peng, J. Li, M. Zhai and Z. Z. Yu, *J. Mater. Chem.*, 2012, **22**, 13064-13069.

23. J. Shen, B. Yan, M. Shi, H. Ma, N. Li and M. Ye, *J. Mater. Chem.*, 2011, **21**, 3415-3421.

24. G. T. S. How, A. Pandikumar, H. N. Ming and L. H. Ngee, *Sci. Rep*., 2014, **4:5044**, 1-8.

25. Y. N. Singhbabu, P. Kumari, S. Parida, R. K. Sahu, *Carbon*, 2014, **74**, 32-43.

26. Y. Liu, *RSC Adv*., 2014, **4**, 36040-36045.

27. A. Ramadoss, G. S. Kim and S. J. Kim, *CrystEngComm*, 2013, **15**, 10222–10229.

28. S. Yang, W. Yue, D. Huang, C. Chen, H. Lin and X. Yang, *RSC Adv.*, 2012,**2**, 8827-8832.

29. S. K. Cheung, N.W. Cheung, *Appl. Phys. Lett*., 1986, **49**, 85.

30. J. Y. Park, H. Lee, J. R. Renzas, Y. Zhang and G. A. Somorjai, *Nano Lett.*, 2008, **8 (8)**, 2388–2392.

31. R. K. Gupta and F. Yakuphanoglu, *Sol. Energy,* 2012, **86**, 1539–1545.

32. M. Soylu, B. Abay, *Physica E Low Dimens. Syst. Nanostruct*., 2010, **43**, 534–538.

33. A. Dey, A. Layek, A. Roychowdhury, M. Das, J. Datta, S. Middya, D. Das and P. P. Ray, *RSC Adv.*, 2015, **5**, 36560–36567.

34. M. D. Stamate, *Appl. Surf. Sci.*,2003, **218**, 317-322.

35. S. Middya, A. Layek, A. Dey, J. Datta, M. Das, C. Banerjee and P. P. Ray, *Chem. Phys. Lett.,* 2014, **610-611**, 39-44.

36. R. Czerw, B. Foley, D. Tekleab, A. Rubio, P. M. Ajayan and D. L. Carroll, *Phys. Rev. B***,** 2002, **66**, 033408.

37. J. W. G. Wilder, L. C. Venema, A. G. Rinzler, R. E. Smalley and C. Dekker, *Nature,* 1998, **391**, 59-62.

Figure captions:

Fig. 1| (a) SEM image of rGO (b) SEM image of TiO_2 (c) SEM image of rGO-TiO_2 (d) TEM image of TiO_2 and (e) TEM image of rGO-TiO_2

Fig. 2| (a) XRD spectra of rGO, TiO_2 and rGO-TiO_2, (b) Williamson hall plot, (c) FTIR spectra of TiO_2 and rGO-TiO_2 and (d) Raman spectra of TiO_2 and rGO-TiO_2

Fig. 3| (a) XPS survey spectra of rGO-TiO_2 composite, (b) Ti 2p spectrum of the rGO-TiO_2 composite, (c) C 1s spectrum of GO and (d) C 1s spectrum of rGO-TiO_2 composite.

Fig. 4| (a) TGA curves of TiO_2 and rGO-TiO_2 (b) N2 adsorption–desorption isotherm at 77 K for TiO_2 and rGO-TiO_2 (black line for TiO_2 and red line for rGO-TiO_2)

Fig. 5| UV-vis absorption spectra of TiO2 and rGO-TiO_2

Fig. 6| I-V plot for TiO_2 and rGO-TiO_2 under (a) dark (b) photo condition

Fig. 7| Photocurrent versus time (I–t) curves of the Schottky barrier diodes based on TiO_2 and rGO-TiO_2 composite

Fig. 8| dV/dlnI vs I and H(I) vs I curve for TiO_2 and rGO-TiO_2 under (a), (b) dark and (c), (d) photo condition

Fig. 9| log I vs log V plot under (a) dark and (b) photo condition, I vs V^2 plot of SCLC region under (c) dark and (d) photo condition

Fig. 10| (a) Cyclic voltammograms and (b) PL spectra of the samples

Fig. 11| Schematic diagram of electron transfer in rGO-TiO_2 composite network

Table caption:

Table 1| Schottky Diode parameters

Table 2| Charge transport parameters

Figures with captions:

Fig. 1

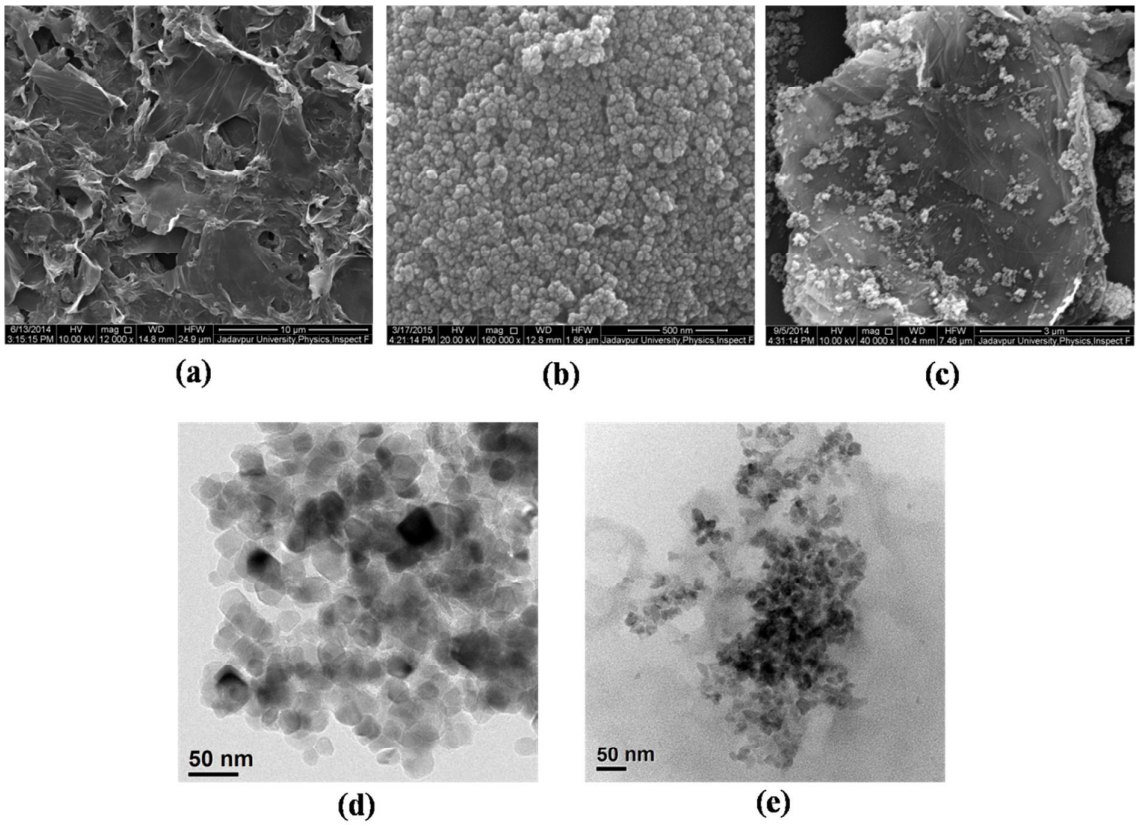

Fig. 1 (a) SEM image of rGO (b) SEM image of TiO_2 (c) SEM image of rGO-TiO_2 (d) TEM image of TiO_2 and (e) TEM image of rGO-TiO_2

Fig. 2

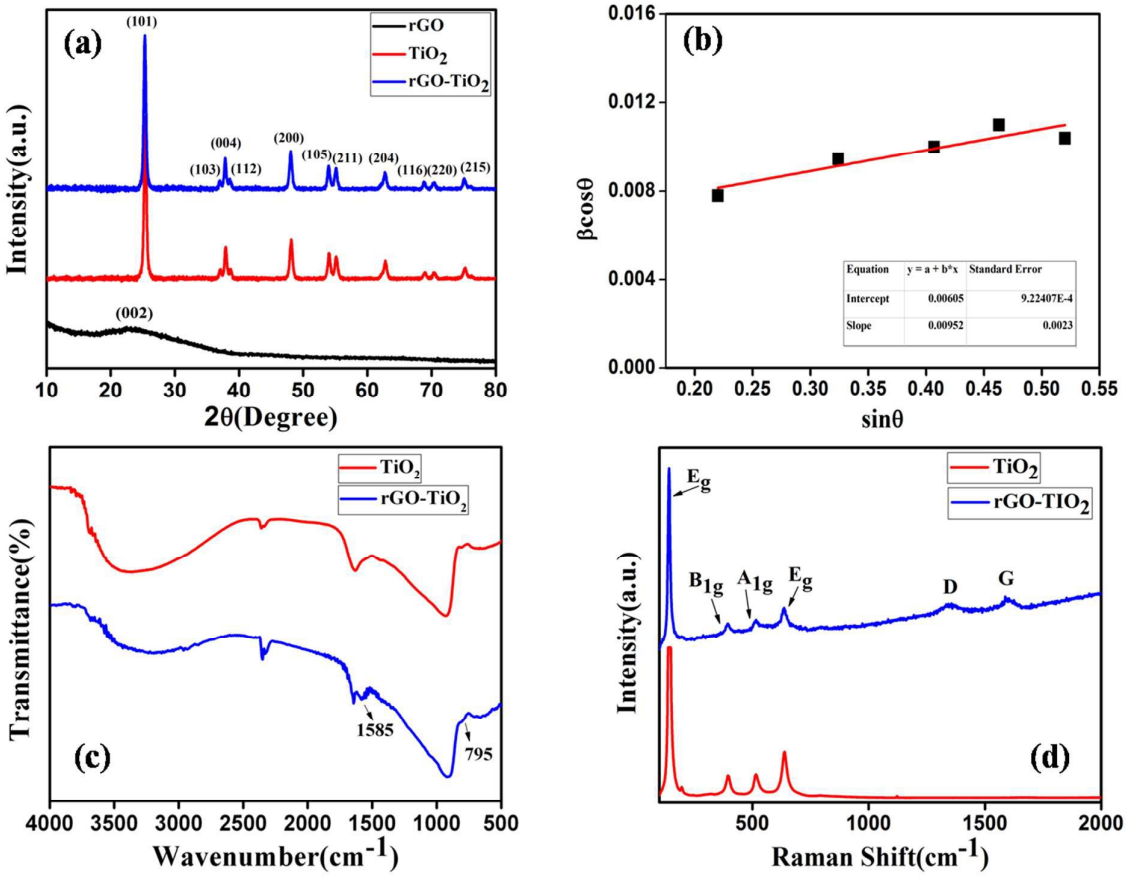

Fig. 2 (a) XRD spectra of rGO, TiO_2 and rGO-TiO_2, (b) Williamson hall plot, (c) FTIR spectra of TiO_2 and rGO-TiO_2 and (d) Raman spectra of TiO_2 and rGO-TiO_2

Fig. 3

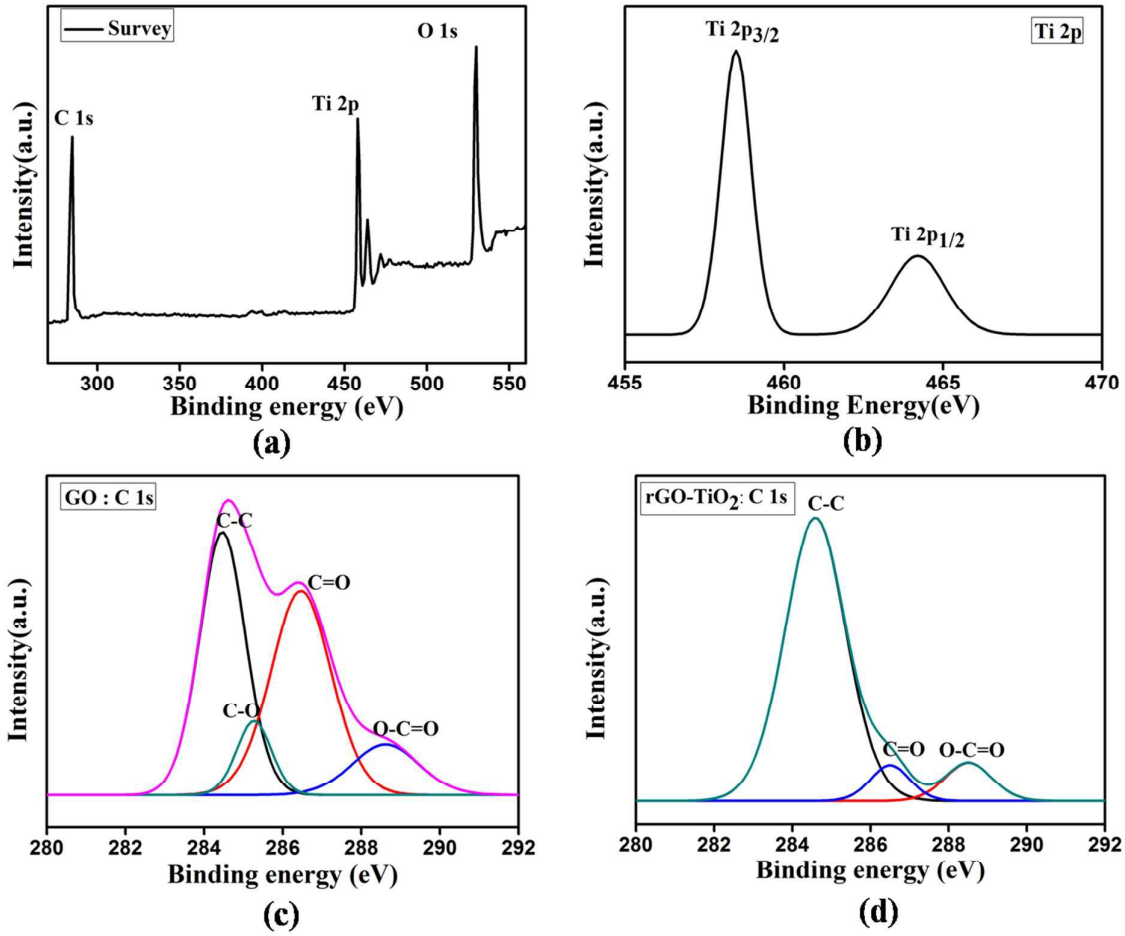

Fig. 3 (a) XPS survey spectra of rGO-TiO_2 composite, (b) Ti 2p spectrum of the rGO-TiO_2 composite, (c) C 1s spectrum of GO and (d) C 1s spectrum of rGO-TiO_2 composite.

Fig. 4

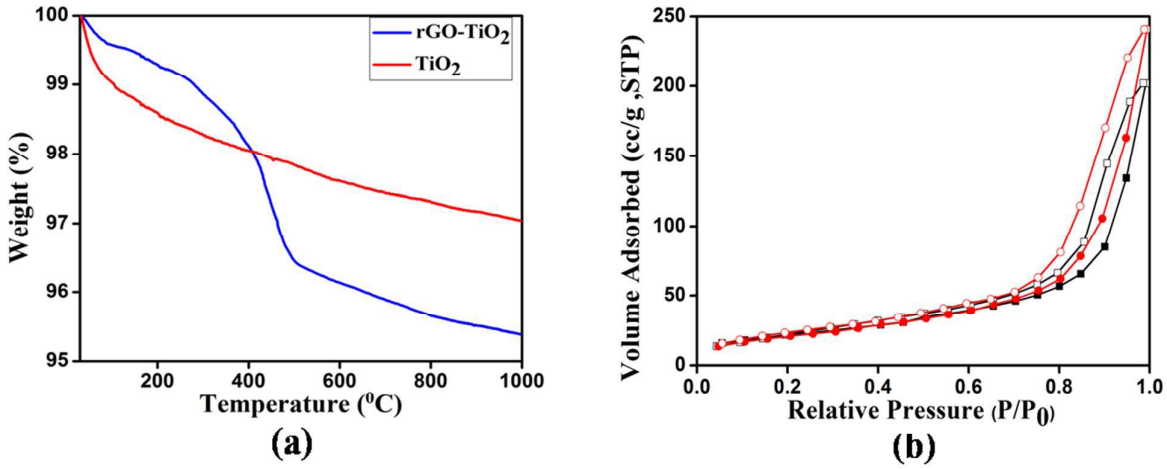

Fig. 4 (a) TGA curves of TiO_2 and rGO-TiO_2 (b) N2 adsorption–desorption isotherm at 77 K for TiO_2 and rGO-TiO_2 (black line for TiO_2 and red line for rGO-TiO_2)

Fig. 5

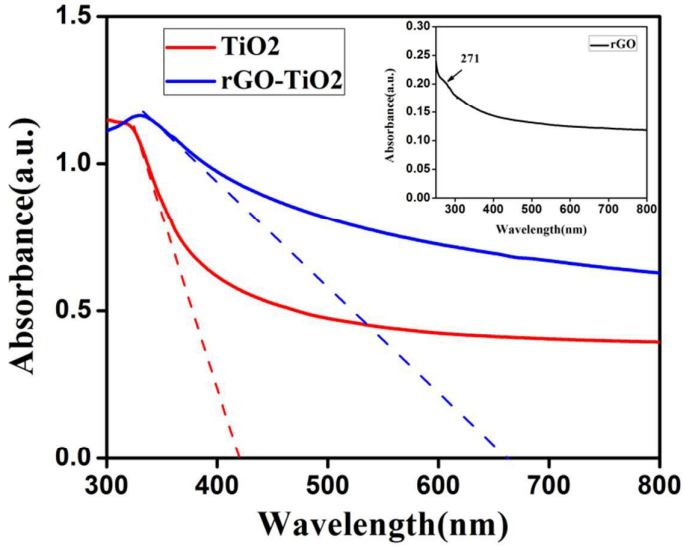

Fig. 5 UV-vis absorption spectra of TiO_2 and rGO-TiO_2

Fig. 6

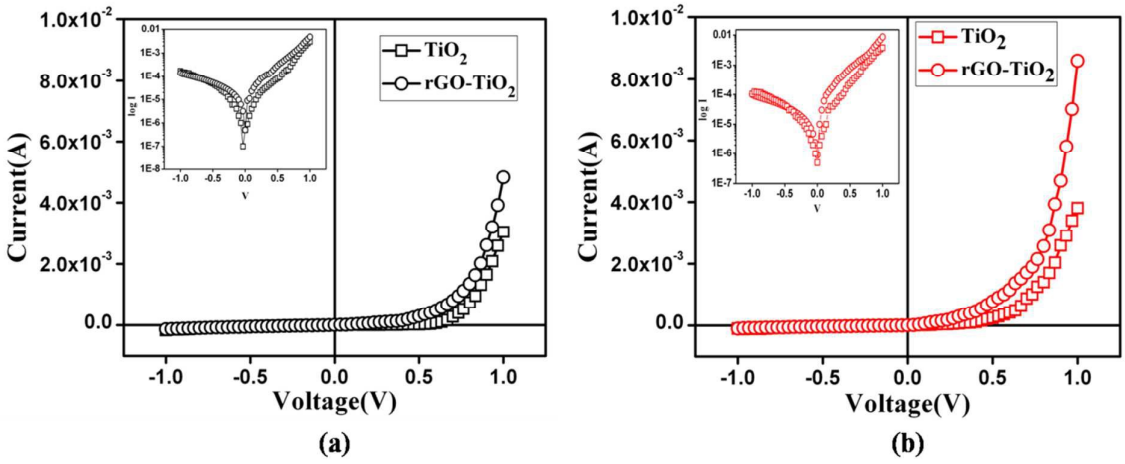

Fig. 6 I-V plot for TiO_2 and rGO-TiO_2 under (a) dark (b) photo condition

Fig. 7

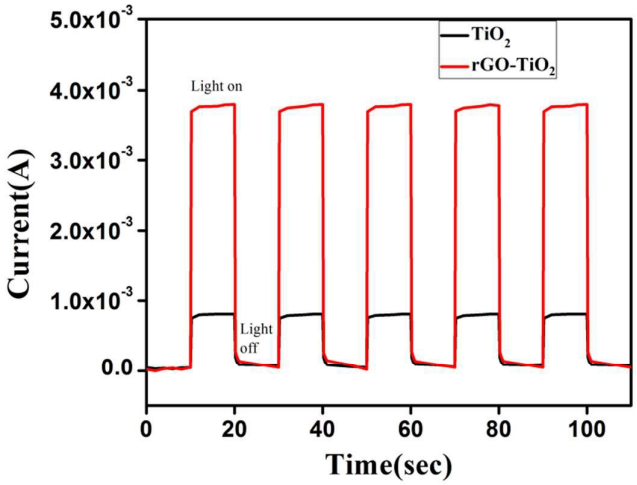

Fig. 7 Photocurrent versus time (I–t) curves of the Schottky barrier diodes based on TiO_2 and rGO-TiO_2 composite

Fig. 8

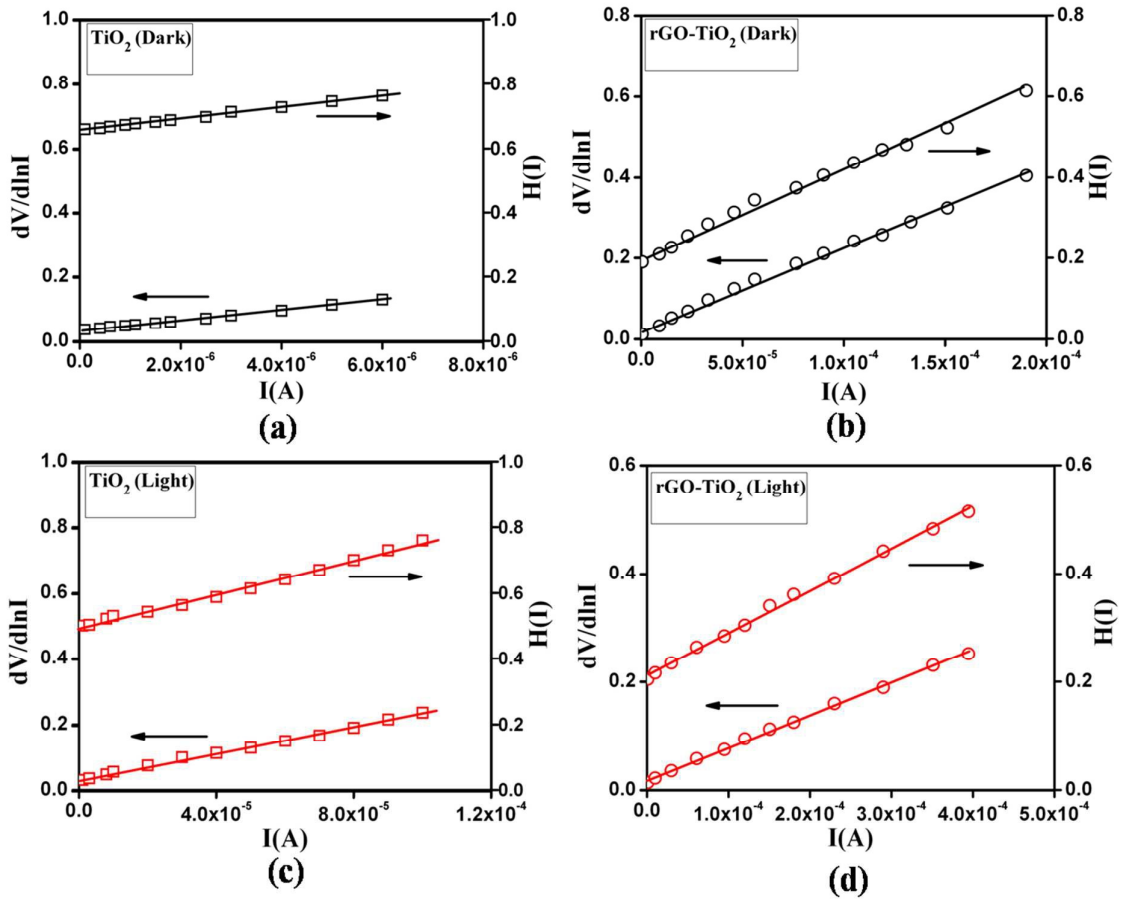

Fig. 8 dV/dlnI vs I and H(I) vs I curve for TiO_2 and rGO-TiO_2 under (a), (b) dark and (c), (d) photo condition

Fig. 9

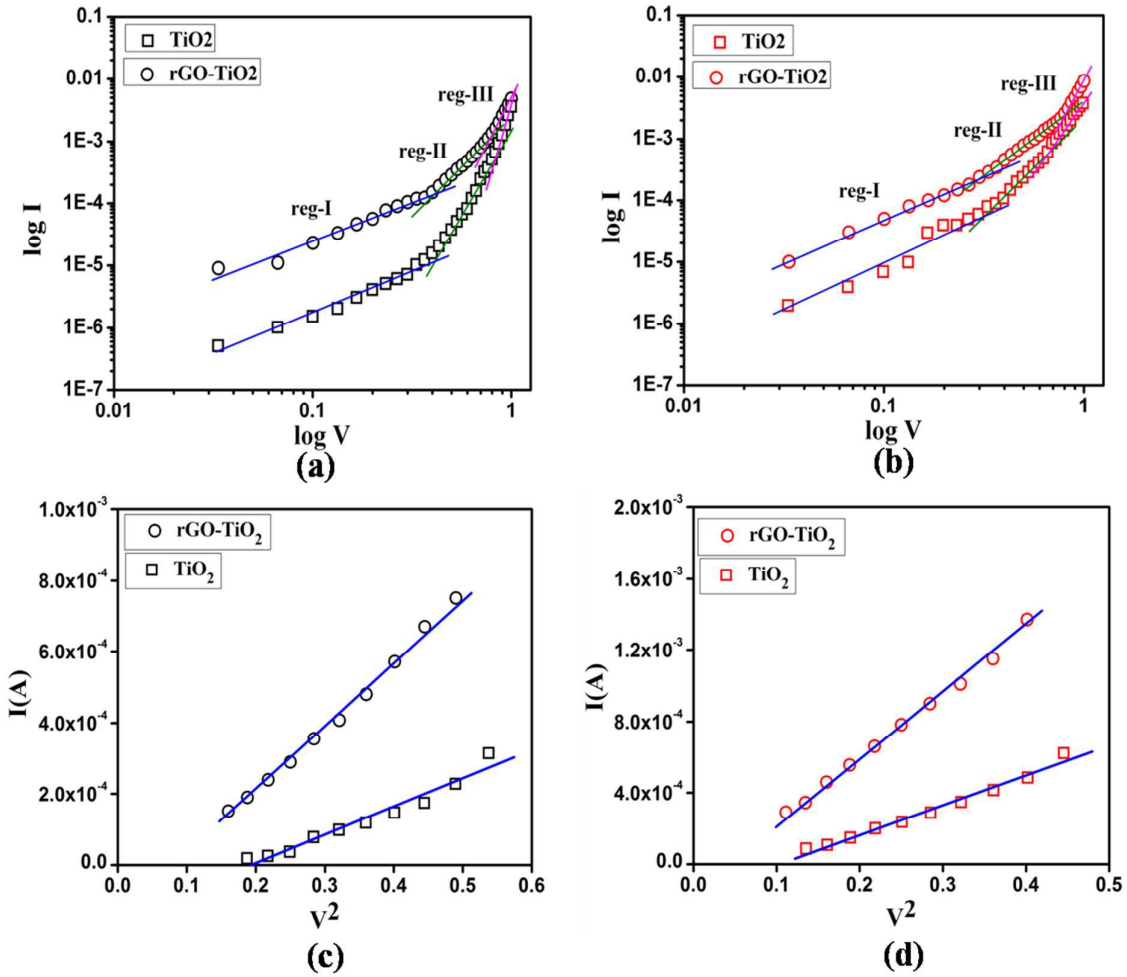

Fig. 9 log I vs log V plot under (a) dark and (b) photo condition, I vs V^2 plot of SCLC region under (c) dark and (d) photo condition

Fig. 10

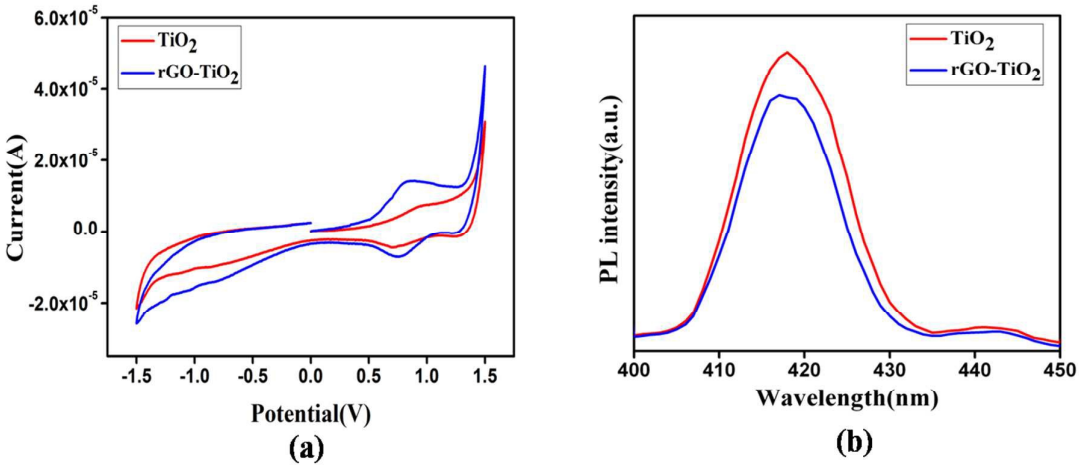

Fig. 10 (a) Cyclic voltammograms and (b) PL spectra of the samples

Fig. 11

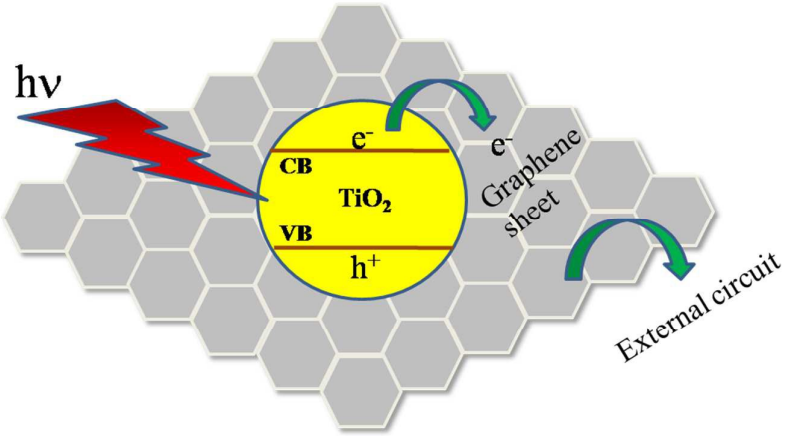

Fig. 11 Schematic diagram of electron transfer in rGO-TiO_2 composite network

Tables with captions:

Table 1

Sample	Cond^{n}.	On/off	Conductivity (S/cm)	Photosensityvity	I.F.	R_S (dv/dlnI) (kΩ)	R_s (H) (kΩ)	φ_b (eV)
rGO-TiO_2	Dark	35	$7.6*10^{-6}$	1.77	0.45	2.07	1.8	0.42
	Light	85	$1.3*10^{-5}$		0.54	0.6	0.74	0.37
TiO_2	Dark	18	$3.8*10^{-6}$	1.26	1.41	15.1	16.9	0.47
	Light	36	$4.8*10^{-6}$		1.2	2	2.7	0.42

Table 1| Schottky Diode parameters

Table 2

Sample	Cond^{n}	$\mu_{eff}*10^{-2}$ ($cm^2\ V^{-1}\ s^{-1}$)	τ (μS)	$\mu_{eff}\tau*10^{-9}$ ($cm^2\ V^{-1}$)	$N_D(*10^{20})$ (m^{-3})	L_D (nm)
rGO-TiO_2	Dark	0.69	1.8	12	68	253
	Light	1.15	1.5	17	71	299
TiO_2	Dark	0.42	2.3	9.66	56	223
	Light	0.52	1.9	9.88	57	230

Table 2| Charge transport parameters